Desalination 377 (2016) 138–151

Contents lists available at ScienceDirect

Desalination

journal homepage: www.elsevier.com/locate/desal

Energy consumption for desalination — A comparison of forward osmosis with reverse osmosis, and the potential for perfect membranes

Nur Muna Mazlan [a], Dimitar Peshev [b], Andrew G. Livingston [a,*]

[a] Imperial College London, UK
[b] University of Chemical Technology and Metallurgy, Sofia, Bulgaria

HIGHLIGHTS

- Custom AspenONE models are developed for quantifying SEC of RO and FO desalination.
- There is no difference in SEC between RO and FO with nanofiltration DS recovery.
- RO competitive with FO despite pressure-driven membrane process for DS recovery
- Infinite membrane permeability does not reduce SEC significantly.
- Advantage of FO derives from lower fouling propensity and specific applications.

GRAPHICAL ABSTRACT

Desalination process flowsheets considered in this study for comparison of SEC.
(A): RO desalination process with UF membrane pretreatment.
(B): FO desalination process with UF membrane pretreatment and varying draw solution recovery methods.

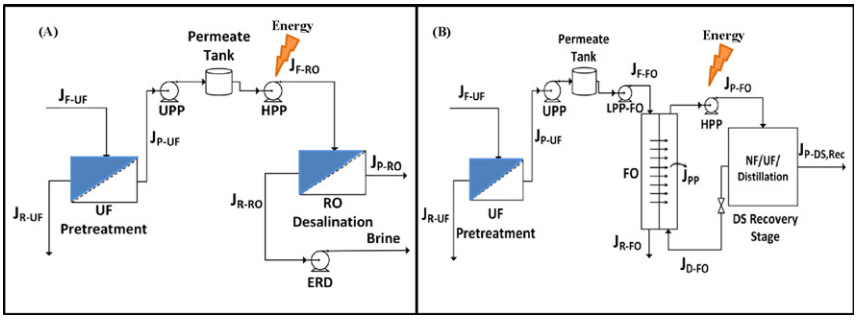

ARTICLE INFO

Article history:
Received 15 June 2015
Received in revised form 14 August 2015
Accepted 17 August 2015
Available online 24 September 2015

Keywords:
Desalination
Energy consumption
Forward osmosis
Reverse osmosis
Membrane processes

ABSTRACT

Reverse osmosis (RO) is now the most ubiquitous technology for desalination, with numerous seawater RO plants being built in water-stressed countries to complement existing water resources. Despite the development of highly permeable RO membranes, energy consumption remains a major contributor to total cost. Forward osmosis (FO) is receiving much attention as a potentially lower energy alternative to RO. However, the draw solution (DS) recovery step in FO requires significant energy consumption. The present study is a modelling approach, simulating FO and RO desalination under various process conditions and process flow schemes using the Aspen Plus environment. Results suggest that there is practically no difference in specific energy consumption (SEC) between standalone RO, and FO with nanofiltration (NF) DS recovery; this can be generalised for any pressure-driven membrane process used for the DS recovery stage in a hybrid FO process. Furthermore, even if any or all of the membranes considered, FO, RO or NF, were perfect (i.e. had infinite permeance and 100% rejection), it would not change the SEC significantly. Hence, any advantage possessed by the FO with NF recovery process derives from the lower fouling propensity of FO, which may reduce or eliminate the need for pretreatment and chemical cleaning.

© 2015 Published by Elsevier B.V.

1. Introduction

Desalination is an attractive technology for the provision of clean water, due to the abundance of seawater. However, it is an energy intensive process compared to other water treatment technologies and poses

* Corresponding author.
E-mail address: a.livingston@imperial.ac.uk (A.G. Livingston).

http://dx.doi.org/10.1016/j.desal.2015.08.011
0011-9164/© 2015 Published by Elsevier B.V.

an environmental challenge in terms of brine discharge. Since the 1970s, seawater reverse osmosis (SWRO) has been the leading technology for seawater desalination, and over this period there has been a large improvement in SWRO energy consumption, from as much as 20 $kWh \cdot m^{-3}$ in the 1970s to nearly 2 $kWh \cdot m^{-3}$ at 50% recovery, now [1]. The practical minimum energy for desalination of seawater at 50% recovery is 1.56 $kWh \cdot m^{-3}$ [1], which suggests potential for further improvement. Recently, forward osmosis (FO) has been receiving increasing interest from academia and industry as a potentially lower energy alternative to SWRO. Given that energy consumption makes up a major portion of the SWRO cost, reaching as high as ~45% of the total permeate production cost [2], it is useful to take a step back and compare the practical energy needs for RO and FO, where FO employs various draw solution recovery methods.

There have been recent publications comparing the energy consumption of a standalone RO process with FO–RO hybrid process for desalination [3,4]. However these studies presented a thermodynamic comparison assuming idealised conditions, and without considering process details such as pressure drop and pretreatment. In this present study, we carry out a more detailed comparison taking the process factors into account. Furthermore, previous comparisons were limited mainly to the FO–RO hybrid process which our study has extended to include other potential draw solution recovery processes. We also carry out a detailed analysis on the potential improvements in membrane permeance on the specific energy consumed and specific membrane area requirements for the various systems, another factor not considered in previous studies.

Published research on SWRO has investigated reducing the SEC by optimising the membrane module [2,5–13] and/or using more permeable membranes [8,14–16]. However, these studies have utilised modelling tools [1,2] without process simulation tools. Most often pre-treatment energy requirements and pressure losses (if included at all in these previous studies) were adopted from other publications or plant data, rather than being quantified by the studies themselves [1,17–19]. Therefore, endogenous calculations on the effects of pretreatment and pressure losses in SWRO are in high demand.

For FO, the main direction of current research is towards improving intrinsic and transport properties of membranes on a molecular level [20–28]. However, the effects of these improvements on the energy efficiency of different FO desalination processes remain unexplored. Consequently, literature lacks comparative data on the SEC of different FO draw solution recovery processes, and how these compare with RO.

To reduce the sources of "side" factors which might compromise the comparison between RO and FO desalination, this present work utilises a unified process simulation environment, providing consistent numerical tolerances and sets of thermodynamic and physical properties models (in particular those embedded in the so called "Electrolytes NRTL" Property Method, available in Aspen's physical properties system) for all simulations. The mathematical models for all custom (non-library) unit operations were programmed in Matlab R2012b, and embedded in the Aspen Plus V7.3 environment. The interoperability between the modelling tool, Matlab, and the process simulation suite, Aspen One, was achieved using CAPE-OPEN interface standards, according to the methodology proposed in [29]. To the best knowledge of the authors, this is the first study which utilises Aspen Plus for simulation of FO and RO desalination processes using custom Matlab models. This customised process simulation approach allows for consistent evaluation and comparison of the energy requirements of FO and RO desalination along with the pretreatment stages, taking into consideration the effects of process configuration, the thermodynamic restriction, product water recovery, draw solution recovery, membrane permeance, applied pressure, draw solution concentration, external and internal mass transfer coefficients, pressure drop and the use of energy recovery devices.

Accordingly, the objectives of the present study are:

i) To quantify and compare SEC for desalination by RO and FO, considering for RO a range of process flow diagrams which account for the effects of pretreatment stages and pressure loss in the membrane modules, and for FO various draw solution recovery options;
ii) To evaluate the potential for improvements in membrane permeance and rejection to reduce the SEC for both RO and FO.

2. Process modelling and simulation

2.1. Process flow diagrams and unit operations

Fig. 1(A) and (B) show the two types of desalination processes that were investigated in this study:

A) Reverse osmosis (RO) with ultrafiltration (UF) pretreatment;
B) Forward osmosis (FO) with UF pretreatment and varying draw solution (DS) recovery methods, namely (a) NF for the recovery of $MgSO_4$ draw solution; (b) UF for the recovery of polyacrylic acid-nanoparticles (PAA-NP) and; (c) distillation for the recovery of CO_2–NH_3 draw solution.

In this study, the energy consumption of SWRO is simulated at various recoveries. Results obtained are compared with simulation of FO to assess if FO has the potential for energy savings compared to RO. A fixed total pure water flowrate of 666 $m^3 \cdot h^{-1}$ (16,000 $m^3 \cdot d^{-1}$), emulating a medium sized desalination plant is used as a basis for calculation. A higher product recovery ratio reduces the total volume of feed water to be pretreated (and hence the cost of pretreatment), whilst maintaining the permeate flowrate. At higher recoveries, less seawater is discharged in the retentate and more is collected as the product water [30].

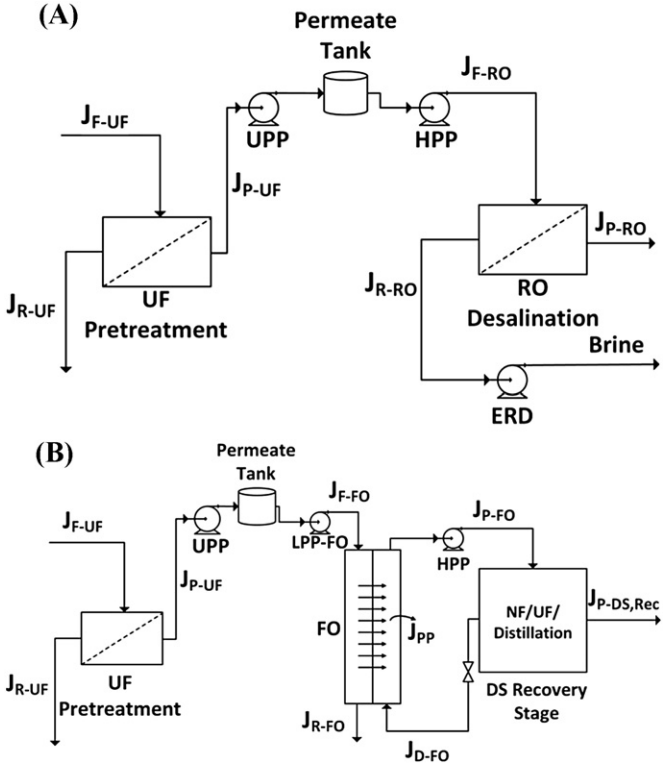

Fig. 1. Desalination process flowsheets considered in this study for comparison of SEC. (A): RO desalination process with UF membrane pretreatment. (B): FO desalination process with UF membrane pretreatment and various draw solution (DS) recovery methods.

2.2. Process models

2.2.1. RO desalination

To estimate practical energy consumption for RO desalination operated near the thermodynamic limit ($\Delta P = \Delta\pi_{exit}$ at the exit of the RO pressure vessel) we construct a model with user specified parameters and calculated variables. User specified parameters include pure water permeance (L_p), corrected van't Hoff factor (∅), applied pressure difference (ΔP), rejection (R), mass transfer coefficient (k), membrane area (A_m), and operating temperature (T). Calculated variables include permeate and retentate flowrates (Q_P and Q_R), permeate and retentate concentrations, osmotic pressure difference between feed and retentate (Δπ), energy consumption of high pressure pumps (HPP) and performance of energy recovery devices (ERD).

A model was developed to simulate the recovery of pure water from seawater at an initial salt concentration of 35 kg·m^{-3}. HPP and ERD efficiencies were user selected. The governing equation used to calculate the permeate flowrate in RO is:

$$Q_P = \frac{L_P A_m (\Delta P(x) - \Delta\pi(x))}{v_P}. \quad (1)$$

NaCl rejection is assumed at 100%. Δπ was estimated using the corrected van't Hoff equation i.e. $\Delta\pi = \varnothing\left(\frac{X_{M,NaCl}}{v_M} - \frac{X_{P,NaCl}}{v_P}\right)R_gT$ where ∅ = 1.64 for a NaCl solution. ∅ is the corrected van't Hoff factor which is a product of the van't Hoff factor and the osmotic coefficient obtained from standard tables (Robinson and Stokes, 1959) [31,32]. A constant value for this factor was assumed, averaged over the range of concentrations of solutions used in this work. The complete set of model equations is listed in Appendix A.

2.2.1.1. Pretreatment effects. Pretreatment is used to produce high quality feedwater for stable and reliable performance in the RO stage.

A model for the RO desalination pretreatment step was developed to calculate the energy consumption of a submerged ultrafiltration (UF) pretreatment unit (Fig. 3(A)). The governing equation used to calculate permeate flowrate is shown in Eq. (1). A membrane permeance of 3.9×10^{-10} m^3·m^{-2}·Pa^{-1}·s^{-1} based on the UF ZeeWeed® 1000 membrane was selected for use in the simulation, along with the assumption that the membrane was 100% permeable to NaCl. Membrane pretreatment was selected over conventional pretreatment given its lower sensitivity to fluctuations in feed water quality, and its ability to guarantee a low silt density index (SDI), therefore enabling operation with high and stable permeate flux over the long-term [18]. A backwash pump was included along with the assumption that the backwash flux is double the UF permeate flux, and that pressure used for backwash (1.6 bar) is double that of the low pressure (0.8 bar absolute) vacuum used to draw water through the pores of the UF fibres. Energy consumption by aeration during filtration was assumed to be ~40% of the total energy consumed by the UF pretreatment unit [33].

The energy consumed by the pretreatment stage is included in SEC calculations for comparison between RO and FO desalination.

2.2.1.2. Pressure drop effects. The energy consumption for SWRO is a function of the applied pressures and feed flowrates, which in turn are dependent on product recovery, plant configuration and frictional losses. Pressure drop across the SWRO module is a parameter which critically influences the transmembrane driving force and, hence, the applied pressure across the membrane and overall performance of the process. For this reason, the effect of process configuration on pressure drop and energy consumption in SWRO was used to select the configuration which gave minimum SEC, and this minimum SEC was used for comparison with FO desalination.

A plug flow pattern was assumed in order to model the pressure, viscosity and concentration changes along the retentate channel in the SWRO modules. A typical 8-in. by 40-in. spiral wound FilmTec (SW30HR-380) module with ~30 leaves was selected for the simulation. The following underlying assumptions were made:

i) Feed channels in the SW module are flat instead of curved due to the channel thickness being much lower than the module radius.
ii) Pressure loss in the permeate channel is negligible. Given the selected SWRO module and typical transmembrane pressures, the average permeate velocity is low and the pressure drop is insignificant [10]. This means the pressure loss is one dimensional only in the feed side.

A schematic diagram of the flat feed channel is shown in Fig. S-1 of the electronic supplementary information (ESI). The properties of the FilmTec SW30HR-380 module can be seen in Table S-1 of the ESI.

The pressure drop across the module was calculated using a semi-empirical pressure drop equation [34] derived for the SWRO module type of interest, given by:

$$\frac{dP_f}{dx} = \lambda \frac{\rho v_f^2}{2d_h} \quad (2)$$

$$\lambda = K_\lambda 6.23 Re^{-0.3} \quad (3)$$

where P_f is the feed side pressure, ρ the fluid density, v_f is the fluid velocity in the feed channel, d_h is the hydraulic diameter of the feed channel, λ is the friction factor, K_λ is a factor introduced to take into consideration pressure losses in the feed tubes and module fittings, with the average value ($K_\lambda = 2.4$) calculated using data obtained from literature based on field data from a SWRO plant in Portugal [10], and *Re* is the Reynolds number.

Based on the underlying equations and parameter values given in Table S-1 of the ESI, the model for pressure drop was constructed as shown in Appendix B.

2.2.2. FO desalination

The objective of the FO modelling is to model practical energy consumption for FO desalination including the draw solution recovery step based on industrial process conditions, and compare results of various FO–DS recovery processes with SWRO. To do this we construct an FO model with user specified parameters and calculated variables. User specified parameters include pure water permeance (L_p), permeate flowrate (Q_P), corrected van't Hoff factor (∅), applied pressure difference (ΔP), rejection (R), mass transfer coefficient (k) and operating temperature (T). Calculated variables include membrane area (A_m), retentate flowrate (Q_R), permeate and retentate concentrations, osmotic pressure differences (Δπ), energy consumption of high pressure pump (HPP) and energy recovery device (ERD).

In all simulations, the recovery of pure water from seawater at a salt concentration of 35 kg·m^{-3} in a single-stage FO was considered. Counter-current flow was assumed for all FO simulations as it provides slight improvement in flux and reduced cross migration of feed and draw solutes, relative to the co-current mode of operation [35–37]. The commercially available HTI CTA membrane with a pure water permeance of 5.56×10^{-12} m^3·m^{-2}·Pa^{-1}·s^{-1} was selected as the basis for our FO simulations. The transport model used for FO was adopted from McCutcheon et al. [38]. Due to unavailability of FO module specifications for industrial scale desalination processes, the FO stage was modelled by calculating the membrane area required based on a user specified permeate flowrate and percentage recovery. The governing equations used to calculate the membrane area and permeate flowrate in the FO and NF DS recovery stages respectively, are:

FO

$$A_m = \frac{(Q_{PP}) \cdot \ln\left(\frac{\Delta\pi_1}{\Delta\pi_2}\right) \cdot \nu_{H_2O}}{L_P \cdot (\Delta\pi_1 - \Delta\pi_2)}. \quad (4)$$

NF (when used for DS recovery)

$$Q_P = \frac{L_P A_m (\Delta P(x) - \Delta\pi(x))}{v_P}. \quad (5)$$

Whereby, NaCl and $MgSO_4$ rejections are assumed at 100% for FO and NF stage, $\varnothing_{NaCl} = 1.64$ and $\varnothing_{MgSO_4} = 1.2$, respectively. $\varnothing$ is the corrected van't Hoff factor which is a product of the van't Hoff factor and the osmotic coefficient obtained from standard tables (Robinson and Stokes, 1959) [31,32]. A constant value for this factor was assumed, averaged over the range of concentrations of solutions used in this work. The complete set of process equations used in the model is listed in Appendix C.

An 8-in. by 40-in. spiral wound FilmTec (NF90-400) module with an active surface area of 37 m^2 was selected for the NF simulation. Pressure drop effects for the NF stage were calculated using similar principles as used for SWRO, whereby NF module (Dow FilmTec NF90-400) operating conditions were obtained from Dow FilmTec [39].

The FO desalination stage was modelled as a single unit operation with specified inlet and outlet pressures and pressure drop values adopted from Hydration Technology Innovations (HTI) bench-scale module design specifications [40], taking into account the design constraints of these modules. As FO technology is not yet commercially available on an industrial scale and data for scaled up FO modules is not readily available, so we have made reasonable estimates based on laboratory data and the limited manufacturer's data which are available. Where used, the external mass transfer coefficient for the FO simulations is $k = 2 \times 10^{-5}$ m·s^{-1} and the solute resistivity to diffusion within the support layer of the FO membrane is $K = 1.1 \times 10^6$ s·m^{-1}. Where stated, UF pretreatment described in Section 2.2.1.1 was included in the total SEC for FO desalination when comparing with SEC for RO desalination.

2.3. Simulation tools

There have been several studies performed on simulating energy consumption in RO desalination using mathematical models and simulation environments [1,2,41–46], which is not surprising given the wide application of RO in the desalination industry. On the other hand, there are at present no such simulation models and software for FO desalination processes, and so no single piece of software which contains library unit operations for both RO and FO processes together. Fortunately, the CAPE OPEN standards for software interoperability allows for efficient and fast integration of custom models and unit operations in commercially available and open source suites of chemical process simulation software. Hence, we have chosen Aspen Plus as the process simulation software for simulating RO and FO desalination in this study. Further details on the procedure for integrating these models and unit operations in Aspen Plus using CAPE OPEN interface standards can be found in Peshev et al. [29].

3. Results and discussion

3.1. Pretreatment effects

Although increases in either membrane permeance (Section 3.3) and/or the number of stages will decrease the SEC required to achieve a specific product recovery, a fundamental question is whether this reduction is significant when compared to the energy requirements of the pretreatment step. If the energy consumed in the pretreatment step is significant compared to the RO unit, and improving RO membrane permeance provides only marginal improvement in the overall SEC, then there is little economic incentive in trying to improve the RO membrane permeance further. Instead, focus should be towards improving the energy efficiency of the pretreatment and post-treatment stages. The effects of pretreatment in RO desalination are presented in this section.

The simulated energy consumption for the UF unit was ~0.11 kWh·m^{-3}, which compares well with values presented in literature [17,47]. Taking into account other pretreatment stages such as seawater intake and screening etc. [19], the total calculated energy consumption for the pre-treatment stage was 0.25 kWh·m^{-3}. These results are summarised in Table 1.

Therefore, efforts to save energy can be made in the pretreatment stage which consumes energy equivalent to ~13% of that used in RO (assuming $SEC_{RO} = 2$ kWh·m^{-3} i.e. the typical value of SEC for optimal RO desalination operation to date). These efforts include increasing permeance of the UF membranes, and optimising the hollow-fibre UF module to improve hydrodynamics without compromising the mechanical strength of the fibre.

3.2. Selection of optimal process configuration for RO desalination

The lowest energy SWRO configuration for comparison of SEC between RO and FO was selected at various product recoveries. Three SWRO configurations were considered for this purpose (Fig. S-2(A) to Fig. S-2(C) in the ESI) using industrial data and guidelines for designing SWRO processes recommended by Dow FilmTec [39]. Each system configuration was characterised by the number of stages, number of elements per stage and array ratio.

For a product recovery of 50%, a series of eight 35 m^2 elements per pressure vessel (also referred here as the basic process unit) was selected. The pressure drop calculated per pressure vessel with a feed flowrate of $Q_F = 12.85$ m^3·h^{-1} (i.e. 70% of the maximum flowrate specified per module), was 4.31 bar. The profile of feed pressure along the modules in series and the effect of varying Q_F are shown in Figs. S-3 and S-4 of the ESI. Pressure drop across the membrane module increased as a function of fluid velocity in the feed channel. It was also shown that in order to operate the 8″ × 40″ SW30HR-380 module under the pressure drop limit of 1 bar, feed flowrate was limited to 13 m^3·h^{-1} or less.

A comparison of different SWRO system configurations is shown in Fig. 2. The process conditions used for the more efficient configurations selected for 50% and 75% product recoveries are listed in Table S-2 of the ESI. It should be noted that given the maximum module operating pressure of 69 bar, the maximum achievable recovery was ~60%, taking into account pressure loss across the module. However, for simulation purposes, a higher product recovery of 75% was chosen for comparison with data available in literature for FO processes, which is explored further in Section 3.5.

At 50% recovery, axial pressure drop for two-stage RO is higher than single-stage due to 12 elements in series in the former compared to 8 in the latter. However, the SEC does not increase for a two-stage (3:2 array ratio) compared to single-stage, as the additional energy required to overcome pressure drop in the second stage is compensated by the energy savings made by the smaller volumes of feed and retentate brought to a higher pressure in the two stages.

The 2:1 configuration has a higher SEC than the 3:2 configuration because the feed into the second stage of 2:1 has a higher flowrate, hence a higher pressure drop, which leads to a higher applied pressure required to overcome these losses. This is shown in Fig. S-5 of the ESI.

Based on these simulation results, a single stage RO is selected for an SWRO process running at 50% product recovery, and a two-stage 3:2 configuration is selected for 75% product recovery. The ASPEN process flowsheets for these configurations are shown in Fig. 3(B) and (C).

3.3. Energy consumption for SWRO

The ASPEN process flowsheet for single-stage RO with UF pretreatment is shown in Fig. 3(A) and (B). Based on this configuration and

Table 1
Energy consumption for UF membrane pre-treatment for desalination.

Type of pretreatment energy consumption		Value of pretreatment energy consumption (kWh·m^{-3} of RO feed)				
UF pretreatment energy consumption	LPP-UF energy consumed	0.024	=	0.11	=	0.25
	Backwash energy consumed	0.044				
	Aeration energy[33]	0.040				
Other pretreatment energy consumption	Seawater intake[19]	0.084	=	0.14		
	Miscellaneous[19]	0.056				

model equations presented in Appendix A, simulation results obtained for energy consumption are summarised in Table 2.

Data in Table 2 show that the mass transfer coefficient and pump efficiencies affect the total energy consumed by the system. Energy consumption increases as mass transfer coefficient decreases (which can be offset by increasing the effective membrane area), and concentration polarisation (CP) effects become more prominent. Membrane area is represented as the specific membrane area i.e. the membrane area required per $m^3 \cdot h^{-1}$ of permeate produced.

The effect of mass transfer coefficient (k) on SEC and product recovery at 100% pump and ERD efficiencies is shown in Fig. S-6(A) of the ESI. We observed that a decrease in mass transfer coefficient decreased product recovery due to an increase in concentration polarisation effects and consequently caused an increase in SEC. At a product recovery of 50%, the effect of mass transfer coefficient on SEC and membrane area required can be seen in Fig. S-6(B). An increase in mass transfer coefficient minimises the SEC until a limiting value of $k = 1.0 \times 10^{-4}$ m·s^{-1} is reached, after which concentration polarisation effects become almost negligible. Improvement in SEC by up to 8% is possible with an increase in k from current values typical of state-of-the-art SWRO modules. Similarly, an increase in k at a constant SEC decreases the membrane area required until a limiting value of $k = 1.0 \times 10^{-4}$ m·s^{-1} is reached.

An increase in pump and energy recovery efficiencies decreases the energy consumption of the system. The selection of HPP and ERD efficiencies in Table 2 was based on common values found in industrial data. For HPP used in SWRO, efficiencies can range from 30% to 90% [48] depending on the type of pump used. In this simulation, HPP efficiencies of 50% and 90% were chosen for comparison. ERD used for SWRO have efficiencies ranging from 90%–98% [49]. Here, 90% efficiency was selected as the base case, and 100% was chosen for comparison with the base case.

The theoretical thermodynamic minimum energy for desalination (i.e. the separation energy equal in magnitude but opposite in sign to the free energy of mixing) at a recovery of 50% is 1.06 kWh·m^{-3} [1]. The practical minimum energy required (i.e. when $\Delta P \approx \Delta\pi_{exit}$) as predicted by the model at 100% pump and energy recovery efficiencies (excluding pressure drop and CP effects) is 1.37 kWh·m^{-3}. This difference is expected because the system is finite and is not operating as a reversible thermodynamic process. This practical minimum energy for desalination calculated by the model is not far behind the calculated value presented by Elimelech et al. of 1.56 kWh·m^{-3} for 50% recovery of 35 g·L^{-1} NaCl solution at 25 °C and 100% NaCl rejection [1].

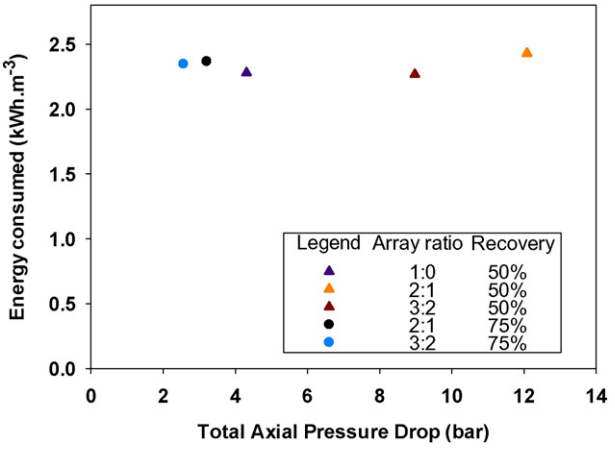

Fig. 2. SEC versus axial pressure drop for different RO system configurations for desalination at 50% and 75% product recovery. The single-stage and two-stage RO consist of 8 and 12 elements in series, respectively. HPP and ERD efficiencies = 100%, $L_p = 3.5 \times 10^{-12}$ m^3·m^{-2}·Pa^{-1}·s^{-1}.

Fig. 4 shows the specific energy consumed versus product recovery calculated with and without an energy recovery device. For the single-stage RO, the theoretical global minimum for energy consumption occurs at a fractional recovery of 50%, as claimed in literature [2]. The specific energy consumption (SEC) of the pump was calculated as follows:

$$SEC_{pump} = \frac{\dot{W}_{pump}}{Q_P} = \frac{Q_F \cdot \Delta P}{Q_P}. \quad (6)$$

At lower recoveries, a higher (SEC) was required to pressurise the feed to a pressure equal to the osmotic pressure at the exit of the module. This is due to the dominating effect of axial pressure drop as a function of higher velocities in the retentate stream (Fig. 5). Higher pretreatment energy consumption due to increased feed flowrates at lower recoveries also contributes to this effect. With increasing product recovery, the SEC decreased due to the effect of decreasing pressure drop and pretreatment energy contribution per unit volume of permeate. However, above a certain recovery (e.g. 35% recovery in Fig. 5), the effects of transmembrane work done by the system began to dominate. A higher rate of increase of ΔP was required to overcome the increasing osmotic pressure, resulting in an increasing SEC with higher recoveries. In the presence of an ERD at 100% efficiency, SEC decreased with decreasing recoveries as energy contained in the retentate was recovered and transferred to the feed. However, at a recovery below 50%, the SEC increases despite the use of an ERD. This is because the effects of pressure drop in the system dominate over energy recovery of the retentate.

At product recoveries below 50%, it is clear that the two-stage RO consumes more energy than the single-stage RO, because it has a higher axial pressure drop. At recoveries below 50%, the higher retentate flowrate entering the second stage led to higher pressure drops and increased SEC compared to the single-stage RO, despite energy savings made due to smaller volumes of water being brought to higher pressures.

Above 50% product recovery, the effects of pressure drop are less significant despite increasing retentate concentration and viscosity, due to the lower retentate flowrate entering the second stage. This results in higher energy savings for the two-stage RO compared to the single-stage RO at product recoveries above 50%.

Fig. 6 shows the specific energy consumption (SEC) of a single-stage RO as the thermodynamic limit ($\Delta P = \Delta\pi_{exit}$) was approached with increasing membrane permeance at 50% recovery, mass transfer coefficient, $k = 4 \times 10^{-5}$ m·s^{-1}, 100% pump and ERD efficiencies. The pressure difference between ΔP and $\Delta\pi_{exit}$ is due to frictional losses. We observed that increasing the membrane permeance from the value typical of state-of-the-art SWRO membranes can improve the SEC by 18%. A recently published paper by Cohen-Tanugi et al. [50] reported a 15% reduction in SEC when the permeance was tripled. Our simulation

Journal Name ARTICLE

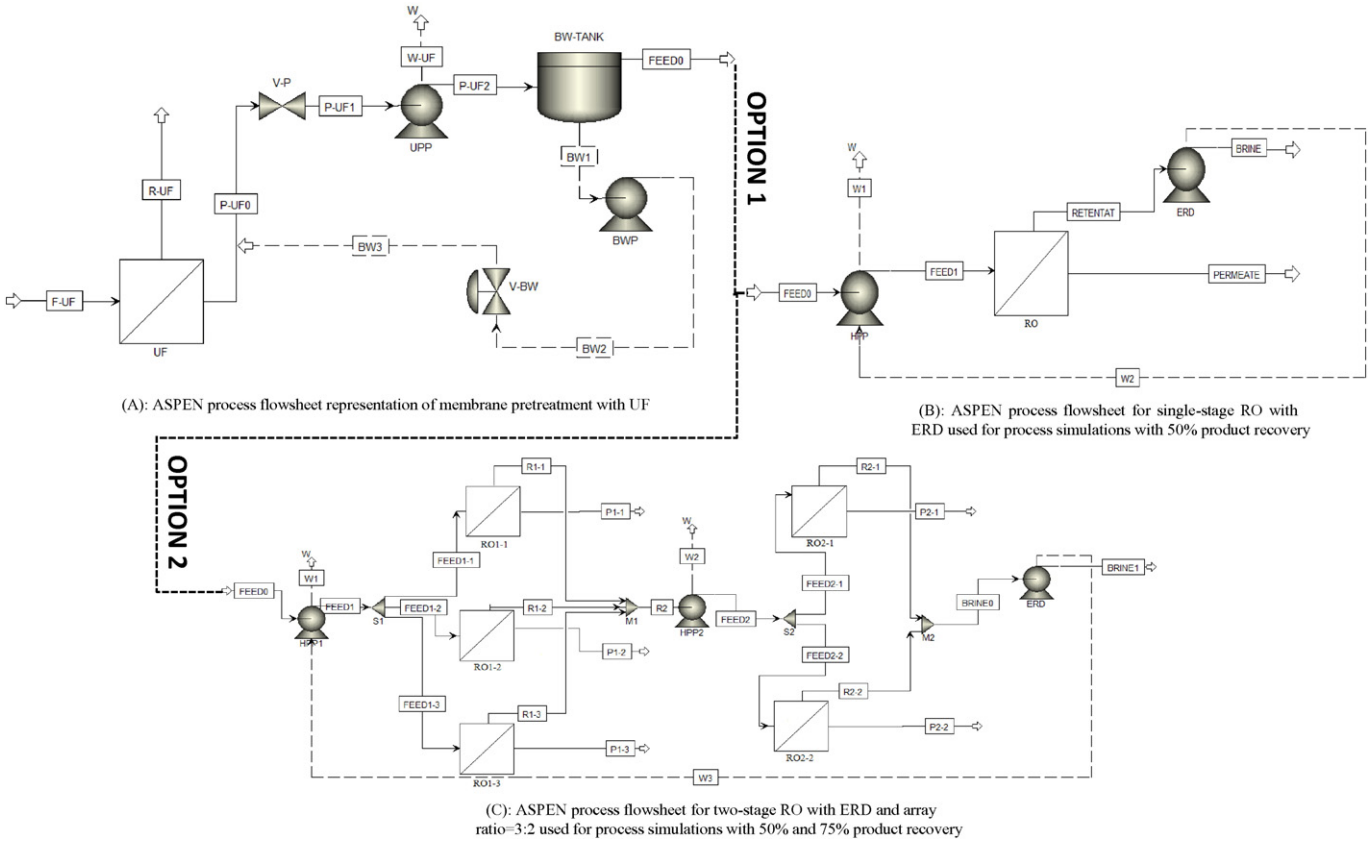

Fig. 3. (A): ASPEN process flowsheet representation of membrane pretreatment with UF. (B): ASPEN process flowsheet for single-stage RO with ERD used for process simulations with 50% product recovery. (C): ASPEN process flowsheet for two-stage RO with ERD and array ratio = 3:2 used for process simulations with 50% and 75% product recovery.

agrees well with this value; however we found that by increasing permeance further i.e. by eight times the current RO permeance, only 18% reduction in the SEC is achievable, after which further increases in permeance did not significantly reduce the SEC of the system.

In the postulated nanoporous graphene membrane simulated by Cohen-Tanugi et al. [51] the best performing pore exhibited full salt rejection and a membrane water permeance of 7.6×10^{-9} $m^3 \cdot m^{-2} \cdot Pa^{-1} \cdot s^{-1}$ (2750 $L \cdot m^{-2} \cdot h^{-1} \cdot bar^{-1}$). However, our simulation suggests that there is a limiting permeance of 2.7×10^{-11} $m^3 \cdot m^{-2} \cdot Pa^{-1} \cdot s^{-1}$ (10 $L \cdot m^{-2} \cdot h^{-1} \cdot bar^{-1}$) near the thermodynamic limit, beyond which the economic incentive for using more permeable membranes is low (i.e. almost negligible) and will decrease with increasing water recovery [52]. However, at conditions near the thermodynamic limit, the use of a more permeable membrane can reduce the amount of membrane area required to achieve the same product recovery (Fig. 6). The system is however limited by concentration polarisation effects which become more limiting at higher permeances due to the increase in permeate flux. As a result, a limiting permeance is observed, beyond which the effects of increasing permeance on membrane area become insignificant. Additionally, operation at higher fluxes would increase concern over fouling and hence the need for more fouling resistant membranes. Contrary to the findings of Cohen-Tanugi et al. [51] using molecular dynamic simulation, whereby computational results suggest that enhanced water permeance of functionalised nanoporous graphene would enable lower energy requirements and lower membrane area requirements, our findings show that the benefits of increasing membrane permeance are limited by the thermodynamic limit and concentration polarisation effects. These findings correspond well to a recent publication by Cohen-Tanugi et al. [50] studying the potential of ultra-permeable membranes in SWRO and brackish water RO.

Data presented for the single-stage RO so far were based on flowrates and process conditions for a SWRO configuration with 8 elements per pressure vessel. In order to scale-up the basic process unit to emulate a medium sized industrial scale process producing 666 $m^3 \cdot h^{-1}$ (16,000 $m^3 \cdot d^{-1}$) of permeate, 104 parallel units are required with a specific membrane area of $A_{m,s} = 43.57$ $[m^2(m^3 \cdot h^{-1})^{-1}]$ as shown in Fig. S-7 of the ESI.

The ASPEN process flowsheet for two-stage RO with UF pretreatment is shown in Fig. 3(A) and (C). The process model results for a two-stage RO with and without an ERD are shown in Fig. 4. It can be seen that the specific energy consumed (SEC) was lower for two-stage RO compared to single-stage RO at product recoveries ≥50%. If an

Table 2
Summary of process calculations for SWRO at a water recovery of 50%, membrane rejection of 100%, $Q_F = 12.85$ $m^3 \cdot h^{-1}$, $\Delta P = 59.5$ bar, $L_p = 3.5 \times 10^{-12}$ $m^3 \cdot m^{-2} \cdot Pa^{-1} \cdot s^{-1}$.

Entry	Mass transfer coefficient, k ($m \cdot s^{-1}$)	η HPP (%)	η ERD (%)	Specific membrane area required $[m^2(m^3 \cdot h^{-1})^{-1}]$	HPP work without ERD (kW)	Net work with ERD (kW)	SEC with ERD ($kWh \cdot m^{-3}$)
1.	4E − 05	50	90	59.14	42.5	33.6	5.3
2.	+∞	50	90	43.57	42.5	33.6	5.3
3.	+∞	90	90	43.57	23.6	14.8	2.3
4.	+∞	50	100	43.57	42.5	32.6	5.1
5.	+∞	90	100	43.57	23.6	13.8	2.2

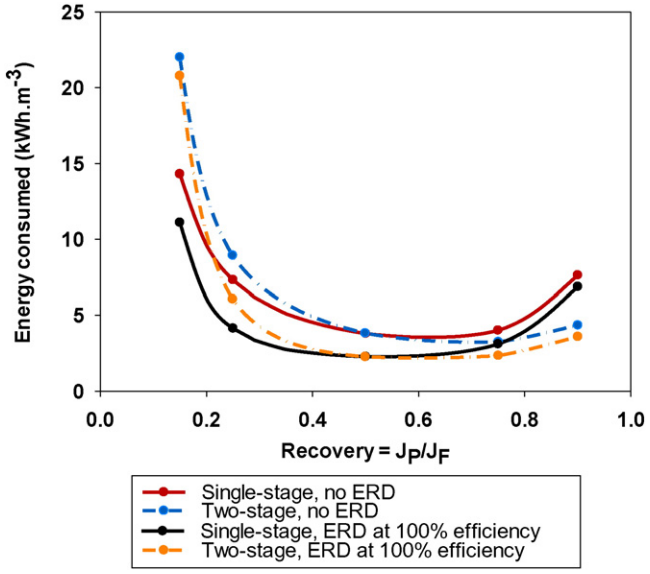

Fig. 4. Specific energy consumed versus product recovery for single-stage and two-stage RO with and without an ERD calculated at HPP efficiency = 100% and k = $+\infty$ m·s^{-1}. Pretreatment energy and effects of pressure drop included.

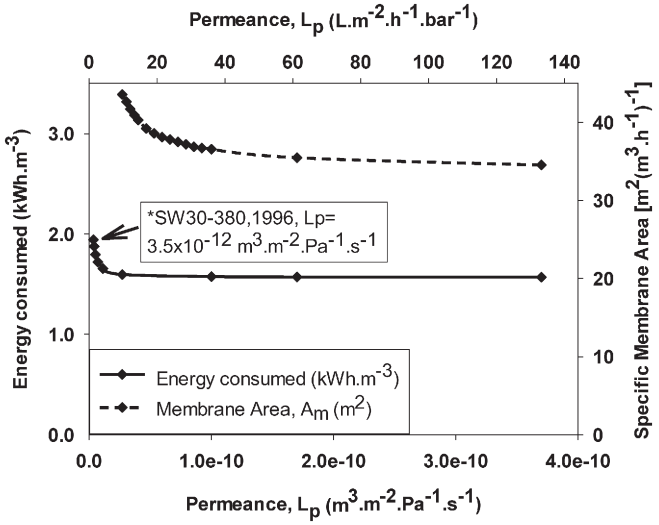

Fig. 6. Change in SEC with increasing membrane permeance as the thermodynamic limit is approached in a single-stage RO at 50% recovery and 100% pump and ERD efficiencies. ΔP was gradually decreased from 65 bar to 53 bar (i.e. near thermodynamic limit, whereby ΔP = 53 bar and $\Delta\pi_{retentate,\ exit}$ = 49 bar). At ΔP = 53 bar and product recovery = 50%, the specific membrane area required is plotted as a function of permeance with k = 4×10^{-5} m·s^{-1}.

infinite number of stages were adopted, this would result in a reversible thermodynamic process with minimum energy consumption for desalination. However, in reality, this system is impractical if the capital costs required are not offset by the energy savings made. A cost analysis of the two-stage RO compared to the single-stage RO is presented in Fig. S-8 of the ESI. The method of calculation used to obtain the overall cost savings for the two-stage RO relative to the single-stage is shown in Appendix D. The dimensionless membrane price, m_{norm} was calculated for seawater based on a study performed by Zhu et al. [2] and details on its derivation are explained further in Appendix D.

The two-stage RO unit with a 3:2 array ratio and 6 elements per pressure vessel used in the SEC comparison with FO for 75% product recovery, can be scaled up to emulate a medium sized industrial process producing 666 m^3·h^{-1} (16,000 m^3·d^{-1}) of permeate. This would require 35 parallel units with a specific membrane area of $A_{m,s}$ = 54.47 [m^2(m^3·h^{-1})$^{-1}$] as shown in Fig. S-9 of the ESI.

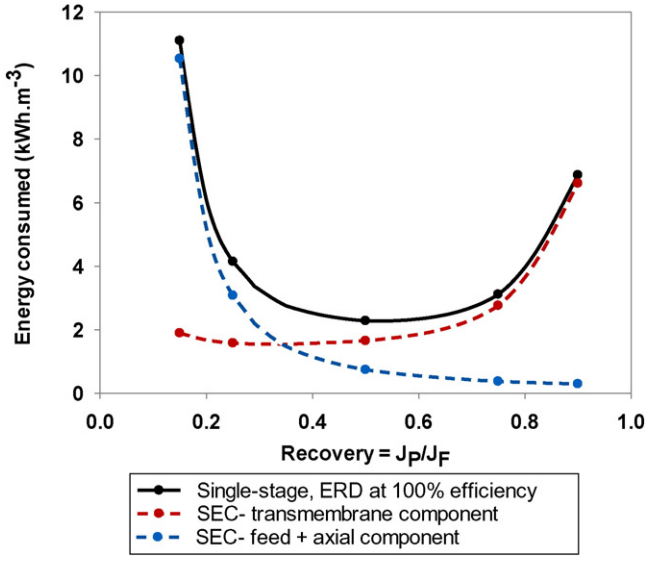

Fig. 5. Contribution of pretreated feed, axial and transmembrane pressure components to SEC in a single-stage RO with ERD at 100% efficiency.

3.4. Energy consumption for FO desalination

The ASPEN process flowsheet for FO desalination followed by NF for recovery of draw solution is shown in Fig. 7. The inlet and outlet pressures for the FO system based on HTI's module design specifications are shown in Fig. 7. The mass transfer coefficients in FO are not yet widely available in the literature. We have estimated values based on reported data for HTI membranes [38,53,54] i.e. k = 2×10^{-5} m·s^{-1} and K = 1.1×10^6 s·m^{-1}, whereby K is the solute resistivity for diffusion within the porous support layer.

Permeate flux in the FO stage is driven by osmotic pressure difference between the feed and draw solutions. Hydraulic pressure is not required in the FO stage other than for recirculation of the feed and draw solutions. The specific energy consumption required for recirculation of feed and draw solutions in the FO stage was estimated for the recirculation pumps using Eq. (6) described in Section 3.3. A "perfect" membrane for FO can be defined as one with infinite permeance, negligible internal concentration polarisation and 100% rejection. At a fixed value for external mass transfer coefficient and solute resistivity for diffusion within the porous support layer of the HTI CTA membrane, the use of a more permeable membrane in FO would reduce the required membrane area for the same target product recovery as shown in Fig. 8(A). However, this decrease in area becomes limited by concentration polarisation effects which become more limiting at high permeabilities. It can be seen that for the currently available HTI CTA membrane, a further increase in membrane permeance has negligible effect on membrane area reduction given that it is already operating under conditions whereby concentration polarisation effects are rate limiting. Hence, further savings in membrane area can only be achieved if the unwanted effects of ICP can be reduced or eliminated. This is shown in Fig. 8(B), whereby keeping the membrane permeance and external mass transfer coefficient constant, a decrease in solute resistivity for diffusion within the porous support layer decreases the required membrane area further until a minimum value is achieved at negligible ICP effects.

We observed that currently available NF membranes such as the Dow FilmTec NF90-400 are already operating near the thermodynamic limit (Fig. 8(C)) and a further increase in membrane permeance has negligible effect on the SEC. The effects of increasing permeance on membrane area are also negligible given that the NF membrane is

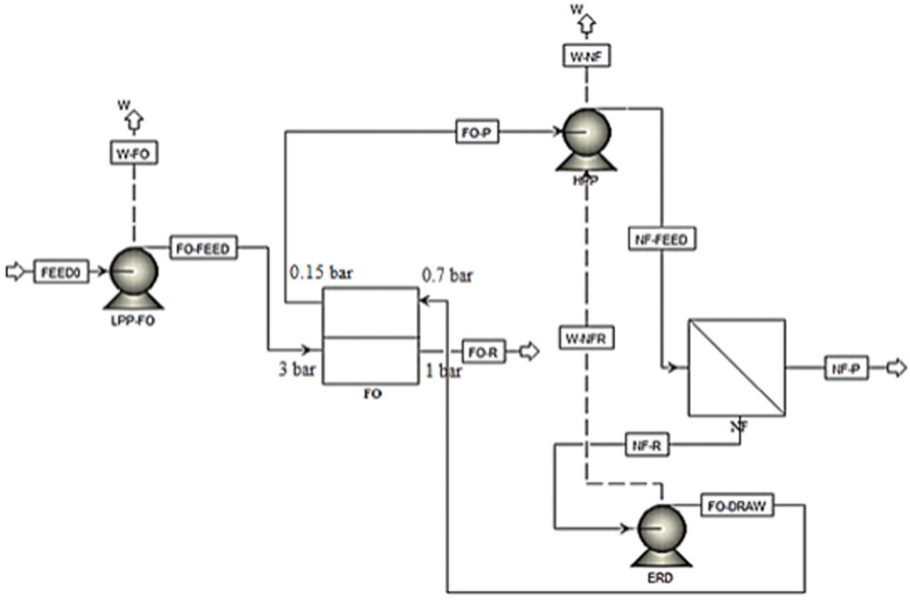

Fig. 7. ASPEN process flowsheet for FO desalination followed by NF for recovery of draw solution. The detailed process configurations are shown in Fig. S-10 (A) and Fig. S-10 (B) in the ESI.

already operating under conditions in which concentration polarisation effects are rate limiting.

3.5. Comparison of energy consumption between FO and RO desalination

Fig. 9 shows a comparison of SEC and specific membrane area between a single-stage RO, FO with NF recovery, FO with two-stage NF recovery, two-stage RO, FO–UF and FO–Distillation at 50% and 75% product recovery. The effects of pretreatment are also taken into account in the energy comparison. The applied pressure, feed and draw solution concentrations used in the various processes shown in Fig. 9, are presented in Table S-3 of the ESI. Results obtained for RO are consistent with those reported in literature [1]. The energy consumption for the FO stage itself is very low e.g. ~0.11 kWh·m^{-3} at 50% recovery because the process is driven by osmotic pressure instead of hydraulic pressure difference and the low pressure pump (LPP) only needs to overcome the pressure drop in the feed channel. At 50% product recovery, the order of membrane processes with the lowest to the highest SEC is *two-stage RO ≤ single-stage RO < FO with two-stage NF recovery ≤ FO with NF recovery*. There is no significant difference in SEC between the FO with NF recovery process and RO at 50% recovery. It should be noted however, that the FO with NF recovery and FO with two-stage NF recovery processes require higher specific membrane areas compared to RO, and this needs to be factored in when performing an overall cost comparison between FO and RO.

At 75% product recovery, there is effectively no difference in SEC between the FO with two-stage NF recovery process compared to a two-stage RO. The FO with CO_2–NH_3 DS recovery process utilising distillation had the lowest SEC compared to all other processes, albeit issues arise with purity of the product water. Key potential advantages of this process include high product recovery (e.g. 75%) at relatively low energy requirements and cost, and brine discharge minimisation. This illustrates that FO hybrid systems can provide energy cost savings for treatment of high salinity feeds if a low-cost thermal energy process is considered for the DS recovery stage [3]. The treatment of high salinity feeds is another advantage of the FO process which cannot be achieved

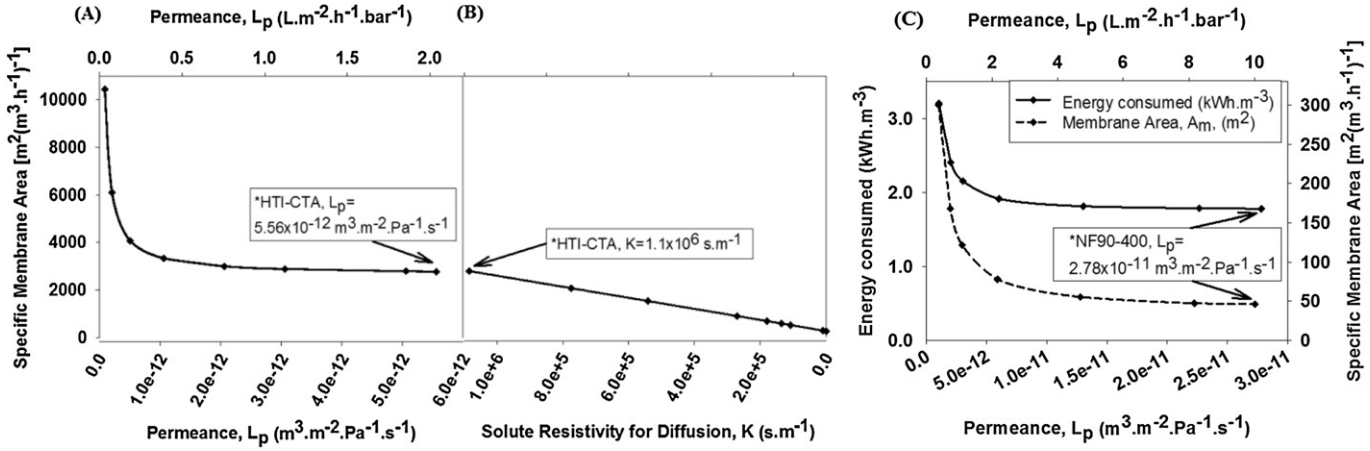

Fig. 8. Effect of increasing membrane permeance and decreasing solute resistivity for diffusion within the FO membrane support layer, on specific membrane area and SEC in a single-stage FO with NF recovery process at 50% product recovery. (A): FO stage — Effect of increasing membrane permeance on specific membrane area required at 50% recovery, $k = 2 \times 10^{-5}$ m.s^{-1} and $K = 1.1 \times 10^{6}$ s·m^{-1}. (B): FO stage — Effect of decreasing solute resistivity for diffusion within the support layer on specific membrane area required at 50% recovery, $k = 2 \times 10^{-5}$ m·s^{-1} and $L_p = 5.56 \times 10^{-12}$ m^3·m^{-2}·Pa^{-1}·s^{-1}. (C): NF stage — Change in SEC with increasing membrane permeance as thermodynamic limit is approached in a single-stage NF at 50% recovery and 100% pump and ERD efficiencies. At a fixed pressure, $\Delta P = 58$ bar (corresponding to pressure near the thermodynamic limit), and recovery = 50%, specific membrane area required is plotted as function of permeance with $k = 4 \times 10^{-5}$ m·s^{-1}.

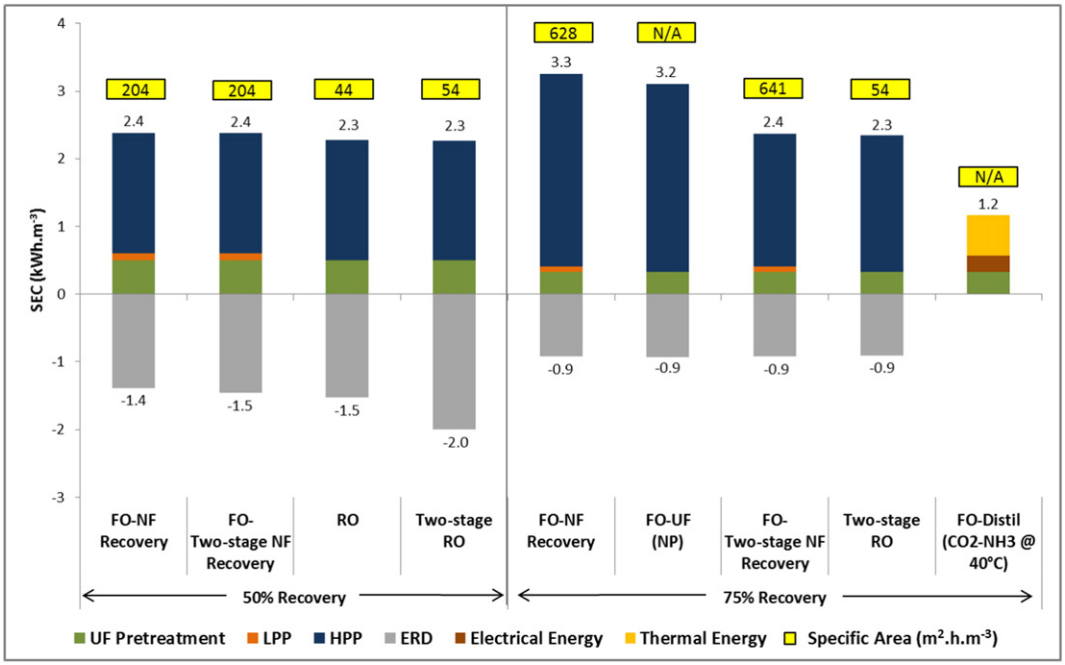

Fig. 9. Comparison of SEC and specific membrane area between FO with NF recovery, FO with two-stage NF recovery, single-stage RO, two-stage RO, FO–UF, and FO–Distillation at 50% and 75% product recovery. Energy contributions from the pretreatment stage, LPP, HPP, ERD and distillation are shown in each process.

in RO due to the limitation of maximum hydraulic pressure in RO modules.

The primary energy input for the CO_2–NH_3 recovery process is for the thermal separation of ammonia and carbon dioxide from the dilute draw solution exiting the FO membrane system. A small amount of electrical energy was used for fluid pumping. The process model and data used for this process was developed by McGinnis et al. using chemical process modelling software (HYSYS, Cambridge, MA) coupled to an electrolyte property package (OLI, Morris Plains, NJ) [55]. Process conditions include 0.5 M NaCl as the feed solution, 5 M ammonium salts (on a CO_2 basis) with a ratio of ammonia to CO_2 of 1.4 as the concentrated draw solution, 1.5 M diluted draw solution as feed to the distillation column, FO operating temperature of 25 °C, reboiler steam temperature of 40 °C, product recovery of 75%. Details on the specifications of the distillation column can be found in McGinnis et al. [55]. A single vacuum distillation column with steam as the heat source for the reboiler gave optimal results for energy consumption. Outputs from this modelling include the heat duty of the distillation column, and power required by the pumps which are expressed in terms of specific equivalent work, W_{eq} (Table 3). Details of the calculation of W_{eq} are presented in McGinnis et al. [55]. The FO with CO_2–NH_3 DS recovery energy data for a single vacuum distillation column is presented in Table 3. It should be noted that all data used in the present work was calculated using our own ASPEN model except for the FO with CO_2–NH_3 DS recovery process, for which data was taken from McGinnis et al. [55].

The total SEC for this process assuming UF pretreatment prior to the FO stage was 1.2 $kWh \cdot m^{-3}$ (Fig. 9). This was much lower than the SEC of RO and FO with NF recovery, although according to the World Health Organisation (WHO) guidelines for drinking water quality [56], the presence of ammonia above 0.2 $mg \cdot L^{-1}$ in water will result in taste and odour problems. It could also lead to decreased disinfection efficiency by chlorine, as 68% of chlorine may react with the ammonia making it unavailable for disinfection. Based on literature [55], product water from the NH_3–CO_2 process may be specified to contain <1 $mg \cdot L^{-1}$ NH_3, however this would still be above the allowable limit of 0.2 $mg \cdot L^{-1}$. The use of waste heat if available, as the heat source instead of steam may reduce the energy consumption of this process further.

Another potential DS is super hydrophilic nanoparticles (NPs) which it is claimed can be recovered efficiently using a 1 kDa UF membrane (FO–UF). It is assumed that recovery with UF will consume considerably less energy in terms of the transmembrane pressures applied compared to RO for DS regeneration [57]. However, the literature lacks actual data on this. A rough calculation of the energy consumption for the FO–UF process illustrated in Appendix E shows that the energy consumed with an ERD at 75% product recovery was 3.2 $kWh \cdot m^{-3}$ assuming UF pretreatment prior to the FO stage. This value is similar to the FO with NF recovery process and significantly higher than the CO_2–NH_3 recovery process (Fig. 9). The energy consumption for FO–UF is also likely to be very similar to a standalone RO and FO–RO process [3]. The reason UF and NF DS recovery systems do not save more energy than RO despite being typically low-pressure processes compared to RO, lies in the limitation posed by the osmotic pressure required for the FO stage at a specific product recovery. At a required product recovery, the hydraulic pressure applied will have to exceed $\Delta\pi$ of the retentate at the exit of a UF, NF or RO module in the DS recovery stage. In the case of NF and UF for draw solute recovery, the requirement for $\pi_{(UF/NF,Brine)} = \pi_{(FO,Draw)}$, negates the low pressure benefits of these systems that would otherwise be attainable in a process whereby osmotic pressure was not limiting and separation was merely based on a sieving mechanism. This analysis can be applied to any pressure-driven membrane process used for the DS recovery stage and corresponds well to the recent

Table 3
FO with CO_2–NH_3 DS recovery energy data for a single vacuum distillation column [55].

Min steam temp. (°C)	Draw solution conc. (M)	Min steam press. (bar)	Heat duty ($MJ \cdot m^{-3}$)	Elec. duty ($kWh \cdot m^{-3}$)	Gained output ratio (GOR)	Equivalent work, W_{eq} ($kWh \cdot m^{-3}$)	Column press. (bar)	Number of stages
40	1.5	0.07	541.55	0.24	4.4	0.84	0.07	1

findings of Shaffer et al. [3]. Modelling energy consumption for the NP recovery stage in ASPEN is challenging as the compounds present, along with their physical and thermo properties, do not exist in the ASPEN databank. A remaining challenge with the FO–UF process is the agglomeration of NPs during draw solution regeneration which reduces permeate flux over time.

A further method which has been proposed for the recovery of draw solution is to use magnetic nanoparticles (MNPs) as a solute and recover them using a magnetic separator generating a magnetic field. At present, there is only one paper by Ge et al. [58] providing data on the power needed for MNP recovery by a magnetic field. This paper mentions the recovery of 50 mL of a magnetic nanoparticle solution in 30 min using a magnetic separator at a power of 187 W. The trapped MNPs were washed away by deionised water after turning off the electromagnet and recycled for use in a fresh draw solution. A simple calculation illustrated in Appendix F shows that an exorbitant amount of energy, i.e. 1870 $kWh \cdot m^{-3}$, was used for the recovery of the MNPs. However, the magnetic separator was not specially designed for the study and only a very small fraction of this energy was consumed by the separation of MNPs [58]. The exact fraction of energy consumed cannot be quantified due to the lack of data in literature at the moment. Hence, the recovery of MNPs with a magnetic separator was not used for comparison in this study but is a potential area for future research.

The order of processes with the lowest to the highest SEC at 75% product recovery is *FO–Distil < two-stage RO < FO with two-stage NF recovery < FO–UF < FO with NF recovery*. There is effectively no difference in SEC between the FO with NF recovery process and RO. Hence, the benefit of the FO with NF recovery process could lie in the reduced fouling propensity of FO [3,59–64] which may reduce or eliminate the need for pretreatment and chemical cleaning, thus reducing costs.

Although 75% product recovery may not be practically feasible due to the pressure limitations of current RO and NF modules, these simulations were performed for purposes of comparison with the FO–Distillation process for which only data at 75% recovery was available in literature.

4. Conclusions

A customised simulation tool was used to estimate the SEC for RO and FO desalination by considering the effect of different process variables and UF pretreatment step. Using a CAPE-OPEN interface standard for running Matlab scripts in ASPEN, this modelling approach provided a flexible tool for quantifying the energy consumption of desalination by simulating real process conditions.

It was concluded that there is effectively no difference in SEC between the FO with NF recovery and RO processes. Furthermore, it has been shown that even if any of the membranes, FO, RO or NF had infinite permeabilities and 100% rejection, it would not change the SEC significantly. Based on these simulations alone, FO with NF recovery cannot be considered to be competitive with RO taking into account the additional capital costs needed for FO with NF recovery, unless other advantages of the process can be capitalised on. One such advantage is the apparently lower fouling propensity of FO [3,59–64] which may reduce or eliminate the need for pretreatment and chemical cleaning, thus reducing costs. In order to investigate if this phenomenon can be exploited, the mechanism and extent of fouling in FO compared to RO needs to be further studied and understood.

The FO–Distillation process with CO_2–NH_3 draw solution showed the lowest SEC compared to other FO and RO desalination processes. However, concerns over residual NH_3 being above the allowable limit in the product water is a challenge which remains to be resolved.

At 75% recovery, the single-stage FO–UF process with NPs as the draw solution is estimated to have a similar SEC to the FO with single-stage NF process. A two-stage UF for the nanoparticle recovery may result in similar SEC as the two-stage RO and FO with two-stage NF recovery processes, albeit increasing capital costs. The lack of data in the literature makes it challenging to model the SEC for this process at varying product recoveries and process conditions. Hence, more research is required in this area to increase the availability of data before accurate comparisons can be made with other desalination processes.

In general, it was observed that despite the type of draw solution and pressure-driven recovery method used, there is effectively no difference in energy consumption of different hybrid FO processes and the standalone RO process. This is because, the requirement for $\pi_{DS\ Recovery,\ Brine} = \pi_{FO,Draw}$ negates the benefit of using draw solutes which can be recovered by low pressure processes. This analysis can be generalised for any pressure-driven membrane process used for the DS recovery stage, although there are still opportunities for hybrid FO processes to provide energy cost savings by leveraging on low-cost thermal energy DS recovery methods such as the FO–Distillation process for recovering the CO_2–NH_3 DS.

Nomenclature

CO_2	carbon dioxide
CP	concentration polarisation
DS	draw solution
ERD	energy recovery device
ESI	electronic supplementary information
FO	forward osmosis
FS	feed solution
HPP	high pressure pump
HTI	Hydration Technology Innovations
LPP	low pressure pump
MBR	membrane bioreactor
MNP	magnetic nanoparticles
NH_3	ammonia
NP	nanoparticles
PAA	polyacrylic acid
PAA-NP	polyacrylic acid-nanoparticles
RO	reverse osmosis
SEC	specific energy consumption
SW module	spiral wound module
SWRO	seawater reverse osmosis
UF	ultrafiltration
UPP	ultrafiltration permeate pump
WHO	World Health Organisation
P	hydraulic pressure (Pa)
π	osmotic pressure, Pa
ΔP	transmembrane pressure difference, Pa
Δπ	osmotic pressure difference across the membrane, Pa
$\Delta\pi_1$	osmotic pressure difference between the permeate and feed side for the FO stage, Pa
$\Delta\pi_2$	osmotic pressure difference between the draw and retentate side for the FO stage, Pa
$\varnothing_{NaCl}$	corrected van't Hoff factor for NaCl solution = 1.64
$\varnothing_{MgSO4}$	corrected van't Hoff factor for $MgSO_4$ solution = 1.2
Q_F	feed flowrate, mol (solvent + solute)$\cdot s^{-1}$
Q_P	permeate flowrate, mol (solvent + solute)$\cdot s^{-1}$
Q_{PP}	pure water permeate flowrate in FO, mol (solvent + solute)$\cdot s^{-1}$
Q_R	retentate flowrate, mol (solvent + solute)$\cdot s^{-1}$
Q_D	draw solution flowrate, mol (solvent + solute)$\cdot s^{-1}$
L_p	membrane permeance, $m^3 \cdot m^{-2} \cdot Pa^{-1} \cdot s^{-1}$
A_m	membrane area, m^2
$A_{m,s}$	specific membrane area, $[m^2(m^3 \cdot h^{-1})^{-1}]$
T	temperature, K
R	membrane rejection, %
R_g	universal gas constant = 8.314 $J \cdot K^{-1} \cdot mol^{-1}$
k	external mass transfer coefficient, $m \cdot s^{-1}$
K	solute resistivity for diffusion within porous support layer, $s \cdot m^{-1}$

X_i molar fraction of the solute
ν_i (P, T, X_i) molar volume of mixtures and solvent as a function of pressure, temperature and molar fractions of the solute, supplied by the thermophysical properties engine, $m^3 \cdot mol^{-1}$
P_f feed side pressure, Pa
ρ fluid density, $kg \cdot m^{-3}$
ν_f fluid velocity, $m \cdot s^{-1}$
d_h hydraulic diameter of the feed channel, m
λ friction factor
K_λ factor to take into consideration pressure losses in the feed tubes and module fittings
W_{pump} pump work, W
W_{eq} equivalent work, $kWh \cdot m^{-3}$
Re Reynolds Number
x position down the feed flow path
Y product recovery
G_{SEC} gain in energy savings
f_{ES} fractional energy savings
P_{SMC} penalty due to the increase in membrane area
m_{norm} dimensionless membrane price
m amortised membrane price per unit area, $Pa \cdot m^3 \cdot m^{-2} \cdot h^{-1}$
m_A amortised membrane unit cost, $£ \cdot m^{-2} \cdot h^{-1}$
β conversion factor, $Pa \cdot m^3 \cdot kWh^{-1}$
ε energy price, $£ \cdot kWh^{-1}$

Acknowledgements

We acknowledge the support provided by the Department of Chemical Engineering, Imperial College London. We also acknowledge the CIMB Regional Scholarship Award awarded by CIMB Foundation (795634-H) to N.M.M.

Appendix A. Process model for RO desalination

$$Q_F - Q_R - Q_P = 0 \tag{A.1}$$

$$Q_F X_{F,NaCl} - Q_R X_{R,NaCl} - Q_P X_{P,NaCl} = 0 \tag{A.2}$$

$$Q_P = \frac{L_P A_m \left[\Delta P - \varnothing\left(\frac{X_{M,NaCl}}{v_M} - \frac{X_{P,NaCl}}{v_P}\right) R_g T\right]}{v_P} \tag{A.3}$$

$$X_{P,NaCl} v_M = X_{M,NaCl} v_P (1 - R) \tag{A.4}$$

$$\frac{X_{M,NaCl}}{v_M} = \left(\frac{X_{R,NaCl}}{v_R} - \frac{X_{P,NaCl}}{v_P}\right) \exp\left[\frac{(Q_P/A_m)v_P}{k}\right] + \frac{X_{P,NaCl}}{v_P}. \tag{A.5}$$

It should be noted that $X_{P,NaCl} = 0$ in the simulation since NaCl rejection is assumed to be 100%. The applied transmembrane pressure, ΔP, is calculated as a function of pressure drop as shown in Appendix B whereby $\Delta P_{(i)} = P_{out(i-1)} - 10^5$(Pa), whereby (i) is the ith element in series down the flow path of the feed.

Appendix B. Model for pressure drop in a typical 8-in. by 40-in. spiral wound FilmTec (SW30HR-380) RO Module [10]

$$\frac{dP_f}{dx} = -2.4 \times 6.23\left(\frac{9.35 \times 10^{-4} \cdot \nu_f \cdot 1025}{\mu}\right)^{-0.3} \frac{1025 \cdot {\nu_f}^2}{2\left(9.35 \times 10^{-4}\right)} = -15.14\left(\frac{\nu_f}{\mu}\right)^{-0.3} \times 548,128.34\, {\nu_f}^2 = -8,300,817 \times \mu^{0.3} \times {\nu_f}^{1.7}$$

$$P_{out}(i) = P_{in}(i+1) = P_{in}(i) - 8,300,817 \cdot c_1\left(\mu(i+1)^{0.3}\right) \cdot c_2\left(\nu_f(i+1)^{1.7}\right) \cdot dx. \tag{A.6}$$

The absolute pressure at the exit of the module, P_{out} i.e. at the exit of the last infinitesimal element, was calculated using Eq. (A.6), whereby c_1 and c_2 are constants. The step size was sufficiently small to ensure no significant effect of its value on the overall pressure drop along the module.

Appendix C. Process model for FO with NF recovery desalination

$$\boldsymbol{A_m} - \frac{Q_{PP} \times v_{H_2O}}{L_P \times \left[\frac{\left[\left[\left(\varnothing_{MgSO_4}\frac{X_{P,MgSO_4}}{v_P} - \varnothing_{MgSO_4}\frac{X_{D,MgSO_4}}{v_D}\right)\exp[-(Q_{PP}/A_m)v_{PP}\cdot K] - \left(\varnothing_{NaCl}\frac{X_{F,NaCl}}{v_F} - \varnothing_{NaCl}\frac{X_{R,NaCl}}{v_R}\right)\exp\left[\frac{(Q_{PP}/A_m)v_{PP}}{k}\right]\right]R_g T\right]}{\left[\ln\frac{\left(\varnothing_{MgSO_4}\frac{X_{P,MgSO_4}}{v_P}\right)\exp[-(Q_{PP}/A_m)v_{PP}\cdot K] - \left(\varnothing_{NaCl}\frac{X_{F,NaCl}}{v_F}\right)\exp\left[\frac{(Q_{PP}/A_m)v_{PP}}{k}\right]}{\left(\varnothing_{MgSO_4}\frac{X_{D,MgSO_4}}{v_D}\right)\exp[-(Q_{PP}/A_m)v_{PP}\cdot K] - \left(\varnothing_{NaCl}\frac{X_{R,NaCl}}{v_R}\right)\exp\left[\frac{(Q_{PP}/A_m)v_{PP}}{k}\right]}\right]}\right] = 0 \tag{A.7}$$

$$Q_P - Q_{PP} - Q_D = 0 \tag{A.8}$$

$$Q_R + Q_{PP} - Q_F = 0 \tag{A.9}$$

$$(X_{R,NaCl} \cdot Q_R) - (X_{F,NaCl} \cdot Q_F) = 0 \tag{A.10}$$

$$(X_{P,MgSO_4} \cdot Q_P) - (X_{D,MgSO_4} \cdot Q_D) = 0 \quad (A.11)$$

Single-stage NF

The process model used for single-stage NF for draw solution recovery is the same as RO (Appendix A) with the NaCl solute in RO replaced by $MgSO_4$ in NF and the corrected van't Hoff factor for the $MgSO_4$ solution is $\varnothing = 1.2$.

Appendix D. Method of calculation used to obtain the gain in energy savings (G_{SEC}) for the two-stage RO relative to the single-stage RO [2]

$$G_{SEC} = \frac{SEC_{1RO}}{\pi_0} f_{ES}$$

where the fractional energy savings,

$$f_{ES} = \frac{SEC(1RO) - SEC(2ROs)}{SEC(1RO)}.$$

The penalty due to the increase in membrane area (P_{SMC}) is calculated using the following Eq. (2)

$$P_{SMC} = \frac{m_{norm}}{\frac{1}{1-Y} - \frac{1}{Y}\ln\left(\frac{1}{1-Y}\right)} \times \left(\frac{A_{mem,1} + A_{mem,2}}{A_{mem,1RO}} - 1\right)$$

where m_{norm} (calculated for desalination as ~0.1) is a dimensionless membrane price which is independent of RO operating conditions calculated using:

$$m_{norm} = \frac{m}{L_p(\pi_0)^2} \times \left(\frac{A_{mem,1} + A_{mem,2}}{A_{mem,1RO}} - 1\right)$$

where m is the amortised membrane price per unit area, given by:

$$m = \frac{m_A \beta}{\epsilon}$$

where m_A ($£ \cdot m^{-2} \cdot h^{-1}$) is the amortised membrane unit cost selected at 100 $£ \cdot m^{-2}$ assuming a membrane life of 5 years, β ($Pa \cdot m^3 \cdot kWh^{-1}$) is the conversion factor calculated as 1.557×10^6 $Pa \cdot m^3 \cdot kWh^{-1}$ and ϵ ($£ \cdot kWh^{-1}$) is the energy price selected at the current average standard price of 0.15 $£ \cdot kWh^{-1}$ [2].

The overall cost savings was calculated as follows:

$$\text{Overall cost savings} = G_{SEC} - P_{SMC}.$$

Appendix E. Calculation of energy consumption for the FO–UF process using nanoparticles (NPs) as the draw solution

Osmotic pressure of 35 $g \cdot L^{-1}$ NaCl = 24.29 bar.

At 75% recovery for FO,

$$\pi_{NaCl,exit} = \frac{24.29}{0.25} = 97.16\,\text{bar}$$

$$\pi_{DS,in} = 97.16 + 2 = 99.16\,\text{bar}$$

$$\pi_{DS,exit} = 99.16 \times 0.25 = 24.79\,\text{bar}.$$

At 75% recovery for UF, $\pi_{\text{reconcentrated NP}} = \frac{24.79}{0.25} = 99.16\,\text{bar}$

$$\Delta P_{required} \approx 100\,\text{bar}$$

$$SEC_{UF} = \frac{\Delta P(Pa) \times 1(h)}{Y \times 3600(s) \times 1000} = \frac{100 \times 10^5(Pa) \times 1(h)}{0.75 \times 3600(s) \times 1000} = 3.70\,kWh \cdot m^{-3}.$$

In the presence of an ERD at 100% efficiency,

$$SEC_{UF,recovered} = \Delta P \times \frac{Q_R}{Q_P} = \frac{100 \times 10^5(Pa) \times \frac{1}{3} \times 1(h)}{3600(s) \times 1000}. = 0.9259\,kWh \cdot m^{-3}$$

Whereby,

$$\frac{Q_R}{Q_P} = \frac{0.25 \times Q_F}{0.75 \times Q_F} = \frac{1}{3} \Rightarrow SEC_{UF,ERD} = 3.7 - 0.9259 = 2.77\,kWh \cdot m^{-3}.$$

Total SEC for FO–UF

$$= 2.77 + 0.07$$
$$= 2.84\,kWh \cdot m^{-3}.$$

Assuming UF pretreatment prior to FO stage with a SEC of 0.33 $kWh \cdot m^{-3}$,

$$SEC_{FO-UF} = 2.84 + 0.33 = 3.2\,kWh \cdot m^{-3}.$$

Appendix F. Calculation of energy consumption for the recovery of MNPs using a magnetic field

$$\text{Permeate flowrate, } Q_P = \frac{50(mL)}{30\ (min)} = 1 \times 10^{-4}\frac{m^3}{h}.$$

SEC

$$= \frac{\text{Magnetic power}}{Q_P} = \frac{187\ (W)}{1 \times 10^{-4}\left(\frac{m^3}{h}\right)} = 1870\,kWh \cdot m^{-3}.$$

Appendix G. Supplementary information

Supplementary information for this article can be found online at http://dx.doi.org/10.1016/j.desal.2015.08.011.

References

[1] M. Elimelech, W.A. Phillip, The future of seawater desalination: energy, technology, and the environment, Science 333 (6043) (2011) 712–717.
[2] A.Z. Zhu, P.D. Christofides, Y. Cohen, Effect of thermodynamic restriction on energy cost optimization of RO membrane water desalination, Ind. Eng. Chem. Res. 48 (13) (2009) 6010–6021.
[3] D.L. Shaffer, et al., Forward osmosis: Where are we now? Desalination 356 (2015) 271–284.
[4] R.K. McGovern, J.H. Lienhard, On the potential of forward osmosis to energetically outperform reverse osmosis desalination, J. Membr. Sci. 469 (2014) 245–250.
[5] S. Avlonitis, W.T. Hanbury, M. Benboudinar, Spiral Wound Modules Performance - an Analytical Solution .1, Desalination 81 (1–3) (1991) 191–208.
[6] S. Avlonitis, W.T. Hanbury, M.B. Boudinar, Spiral wound modules performance — an analytical solution. 1, Desalination and Water Re-use: Proceedings of the Twelfth International Symposium, vol. 1 1991, pp. 191–208 (125).
[7] S.A. Avlonitis, M. Pappas, K. Moutesidis, A unified model for the detailed investigation of membrane modules and RO plants performance, Desalination 203 (1–3) (2007) 218–228.
[8] J. Beca, Pharmaceutical discharge: zero discharge for pharma plant, Filtr. Sep. 44 (6) (2007) 40–41.
[9] M. Benboudinar, W.T. Hanbury, S. Avlonitis, Numerical-simulation and optimization of spiral-wound modules, Desalination 86 (3) (1992) 273–290.
[10] V. Geraldes, N.E. Pereira, M.N. de Pinho, Simulation and optimization of medium-sized seawater reverse osmosis processes with spiral-wound modules, Ind. Eng. Chem. Res. 44 (6) (2005) 1897–1905.
[11] R. Rautenbach, W. Dahm, Design and optimization of spiral-wound and hollow fiber Ro-modules, Desalination 65 (1–3) (1987) 259–275.
[12] W.G.J. van der Meer, J.C. van Dijk, Theoretical optimization of spiral-wound and capillary nanofiltration modules, Desalination 113 (2–3) (1997) 129–146.
[13] A. Villafafila, I.M. Mujtaba, Fresh water by reverse osmosis based desalination: simulation and optimisation, Desalination 155 (1) (2003) 1–13.
[14] K. Fethi, Optimization of energy consumption in the 3300 m(3)/d RO Kerkennah plant, Desalination 157 (1–3) (2003) 145–149.
[15] J.E. Nemeth, Innovative system designs to optimize performance of ultra-low pressure reverse osmosis membranes, Desalination 118 (1–3) (1998) 63–71.
[16] M. Wilf, Design consequences of recent improvements in membrane performance, Desalination 113 (2–3) (1997) 157–163.
[17] E. Cardona, A. Piacentino, F. Marchese, Energy saving in two-stage reverse osmosis systems coupled with ultrafiltration processes, Desalination 184 (1–3) (2005) 125–137.
[18] C. Fritzmann, et al., State-of-the-art of reverse osmosis desalination, Desalination 216 (1–3) (2007) 1–76.
[19] P. Cote, S. Siverns, S. Monti, Comparison of membrane-based solutions for water reclamation and desalination, Desalination 182 (1–3) (2005) 251–257.
[20] N.Y. Yip, et al., High performance thin-film composite forward osmosis membrane, Environ. Sci. Technol. 44 (10) (2010) 3812–3818.
[21] A. Tiraferri, et al., Relating performance of thin-film composite forward osmosis membranes to support layer formation and structure, J. Membr. Sci. 367 (1–2) (2011) 340–352.
[22] K.Y. Wang, R.C. Ong, T.S. Chung, Double-skinned forward osmosis membranes for reducing internal concentration polarization within the porous sublayer, Ind. Eng. Chem. Res. 49 (10) (2010) 4824–4831.
[23] L. Setiawan, et al., Fabrication of novel poly(amide-imide) forward osmosis hollow fiber membranes with a positively charged nanofiltration-like selective layer, J. Membr. Sci. 369 (1–2) (2011) 196–205.
[24] K.Y. Wang, et al., Enhanced forward osmosis from chemically modified polybenzimidazole (PBI) nanofiltration hollow fiber membranes with a thin wall, Chem. Eng. Sci. 64 (7) (2009) 1577–1584.
[25] Q. Yang, K.Y. Wang, T.S. Chung, Dual-layer hollow fibers with enhanced flux as novel forward osmosis membranes for water production, Environ. Sci. Technol. 43 (8) (2009) 2800–2805.

[26] S. Zhang, et al., Well-constructed cellulose acetate membranes for forward osmosis: Minimized internal concentration polarization with an ultra-thin selective layer, J. Membr. Sci. 360 (1–2) (2010) 522–535.
[27] C. Qiu, et al., High performance flat sheet forward osmosis membrane with an NF-like selective layer on a woven fabric embedded substrate, Desalination 287 (2012) 266–270.
[28] C.Q. Qiu, S.R. Qi, C.Y.Y. Tang, Synthesis of high flux forward osmosis membranes by chemically crosslinked layer-by-layer polyelectrolytes, J. Membr. Sci. 381 (1–2) (2011) 74–80.
[29] D. Peshev, A.G. Livingston, OSN Designer, a tool for predicting organic solvent nanofiltration technology performance using Aspen One, MATLAB and CAPE OPEN, Chem. Eng. Sci. 104 (2013) 975–987.
[30] P.I. Water, Available from: http://puretecwater.com/what-is-reverse-osmosis.html#recovery2012–2013.
[31] R.A. Robinson, R.H. Stokes, Electrolyte Solutions; the Measurement and Interpretation of Conductance, Chemical Potential, and Diffusion in Solutions of Simple Electrolytes, 2d ed., xv, Butterworths, London, 1959 (571 pp.).
[32] R. Heyrovska, Physical electrochemistry of strong electrolytes based on partial dissociation and hydration — quantitative interpretation of the thermodynamic properties of NaCl(aq) from "zero to saturation", J. Electrochem. Soc. 143 (6) (1996) 1789–1793.
[33] B.B. Choi, et al., Energy management in submerged microfiltration systems by optimum control of aeration, Desalination 247 (1–3) (2009) 233–238.
[34] G. Schock, A. Miquel, Mass-transfer and pressure loss in spiral wound modules, Desalination 64 (1987) 339–352.
[35] A. Sagiv, et al., Analysis of forward osmosis desalination via two-dimensional FEM model, J. Membr. Sci. 464 (2014) 161–172.
[36] J. Lee, B. Kim, S. Hong, Fouling distribution in forward osmosis membrane process, J. Environ. Sci. (China) 26 (6) (2014) 1348–1354.
[37] S.M. Shim, W.S. Kim, A numerical study on the performance prediction of forward osmosis process, J. Mech. Sci. Technol. 27 (4) (2013) 1179–1189.
[38] J.R. McCutcheon, M. Elimelech, Influence of concentrative and dilutive internal concentration polarization on flux behavior in forward osmosis, J. Membr. Sci. 284 (1–2) (2006) 237–247.
[39] FilmTec, D. Steps to Design an RO/NF Membrane System. Available from: http://www.dowwaterandprocess.com/support_training/literature_manuals/lm_techinfo/designstps.htm.
[40] http://www.htiwater.com/contact/index.html. (cited 2014 13 June).
[41] B.J. Feinberg, G.Z. Ramon, E.M.V. Hoek, Thermodynamic analysis of osmotic energy recovery at a reverse osmosis desalination plant, Environ. Sci. Technol. 47 (6) (2013) 2982–2989.
[42] M.H. Li, Minimization of energy in reverse osmosis water desalination using constrained nonlinear optimization, Ind. Eng. Chem. Res. 49 (4) (2010) 1822–1831.
[43] M.H. Li, Reducing specific energy consumption in Reverse Osmosis (RO) water desalination: an analysis from first principles, Desalination 276 (1–3) (2011) 128–135.
[44] C. Liu, K. Rainwater, L.F. Song, Energy analysis and efficiency assessment of reverse osmosis desalination process, Desalination 276 (1–3) (2011) 352–358.
[45] C. Liu, K. Rainwater, L.F. Song, Calculation of energy consumption for crossflow RO desalination processes, Desalin. Water Treat. 42 (1–3) (2012) 295–303.
[46] B.W. Oi, et al., Operating energy consumption analysis of RO desalting system: effect of membrane process and energy recovery device (ERD) performance variables, Ind. Eng. Chem. Res. 51 (43) (2012) 14135–14144.
[47] M. Wilf, M.K. Schierach, Improved performance and cost reduction of RO seawater systems using UF pretreatment, Desalination 135 (1–3) (2001) 61–68.
[48] W. Technology, [Cited 2013; Available from: http://www.watertechonline.com/articles/what-to-look-for-in-desalination-pumps2010.
[49] F. Corporation, Desalination Bulletin, 2012 [cited 2013; Available from: http://www.flowserve.com/files/Files/Literature/FPD/fpd-10-ea4.pdf.
[50] R.K.M. David Cohen-Tanugi, S.H. Dave, J.H. Lienhard, J.C. Grossman*, Quantifying the potential of ultra-permeable membranes for water desalination, Energy Environ. Sci. 3 (2014) 1134–1141.
[51] D. Cohen-Tanugi, J.C. Grossman, Water desalination across nanoporous graphene, Nano Lett. 12 (7) (2012) 3602–3608.
[52] A.H. Zhu, et al., Reverse osmosis desalination with high permeability membranes — cost optimization and research needs, Desalin. Water Treat. 15 (1–3) (2010) 256–266.
[53] Mutual diffusion-coefficients in aqueous-electrolyte solutions (technical report), Pure Appl. Chem. **65** (12) (1993) 2614–2640.
[54] J.R. McCutcheon, M. Elimelech, Modeling water flux in forward osmosis: implications for improved membrane design, AICHE J. 53 (7) (2007) 1736–1744.
[55] R.L. McGinnis, M. Elimelech, Energy requirements of ammonia-carbon dioxide forward osmosis desalination, Desalination 207 (1–3) (2007) 370–382.
[56] W.H. Organization, Guidelines for drinking-water quality, 2nd ed., vol. 2, 1996 (Available from: http://www.who.int/water_sanitation_health/dwq/ammonia.pdf. March 2013).
[57] M.M. Ling, T.S. Chung, Desalination process using super hydrophilic nanoparticles via forward osmosis integrated with ultrafiltration regeneration, Desalination 278 (1–3) (2011) 194–202.
[58] Q.C. Ge, et al., Hydrophilic superparamagnetic nanoparticles: synthesis, characterization, and performance in forward osmosis processes, Ind. Eng. Chem. Res. 50 (1) (2011) 382–388.
[59] B. Mi, M. Elimelech, Chemical and physical aspects of organic fouling of forward osmosis membranes, J. Membr. Sci. 320 (1–2) (2008) 292–302.
[60] B.X. Mi, M. Elimelech, Organic fouling of forward osmosis membranes: fouling reversibility and cleaning without chemical reagents, J. Membr. Sci. 348 (1–2) (2010) 337–345.
[61] A. Achilli, et al., The forward osmosis membrane bioreactor: a low fouling alternative to MBR processes, Desalination 239 (1–3) (2009) 10–21.
[62] S. Lee, et al., Comparison of fouling behavior in forward osmosis (FO) and reverse osmosis (RO), J. Membr. Sci. 365 (1–2) (2010) 34–39.
[63] H.S. Peter Nasr, Forward osmosis: an alternative sustainable technology and potential applications in water industry, Clean Techn. Environ. Policy (2015).
[64] Y.L. Liu, B.X. Mi, Combined fouling of forward osmosis membranes: synergistic foulant interaction and direct observation of fouling layer formation, J. Membr. Sci. 407 (2012) 136–144.